LHCb anomaly in $B \to K^* \mu^+ \mu^-$ optimised observables and potential of Z' model

Ishtiaq Ahmed[1)] Abdur Rehman[2)]

National Centre for Physics, Quaid-i-Azam University Campus, Islamabad, 45320 Pakistan

Abstract: Over the last few years LHCb found some discrepancies in $b \to s l^+ l^-$ FCNC transitions, including anomalies in the angular observables of $B \to K^* \mu^+ \mu^-$, particularly in P_5', in the low dimuon mass region. Recently, these anomalies have been confirmed by Belle, CMS and ATLAS. As direct evidence of physics beyond the Standard Model is absent so far, these anomalies are being interpreted as indirect hints of new physics. In this context, we study the implications of the family non-universal Z' model for the angular observables $P_{1,2,3}$, $P'_{4,5,6}$ and newly proposed lepton flavor universality violation observables, $Q_{4,5}$, in the $B \to K^*(\to K\pi)\mu^+\mu^-$ decay channel in the low dimuon mass region. To see the variation in the values of these observables from their Standard Model values, we have chosen different scenarios for the Z' model. It is found that these angular observables are sensitive to the values of the parameters of the Z' model. We have also found that with the present parametric space of the Z' model, the P_5'-anomaly could be accommodated. However, more statistics on the anomalies in the angular observables are helpful to reveal the status of the considered model and, in general, the nature of new physics.

Keywords: FCNC, new physics, semileptonic B meson decays

PACS: 13.20 He, 14.40 Nd **DOI:** 10.1088/1674-1137/42/6/063103

1 Introduction

In flavor physics, the study of rare B meson decays provides us with a powerful tool, not only to test the Standard Model (SM) at loop level but also to search for possible new physics (NP). Searching for NP in rare decays of B-meson demands that we focus on those observables which contain minimum hadronic uncertainties, such that they can be predicted precisely in the SM and are available at current colliders. In exclusive rare B meson decays, the main source of hadronic uncertainties come from the form factors, which are non-perturbative quantities and are difficult to compute. In addition, these uncertainties may preclude the signature of any possible NP. From this point of view, among all rare decays, the four body decay channel, $B \to K^*(\to K\pi)\mu^+\mu^-$, is of special interest because it gives a large variety of angular observables, namely, P_i (i=1,2,3) and P_i' (i=4,5,6) [1] which are free from hadronic uncertainties [2]. The comparison between the theoretical predictions of these kind of observables in the SM with the experimental data could be helpful to clear some smog on physics beyond the SM.

From the experimental point of view, a few years back LHCb measured the values of these angular observables for the decay channel $B \to K^*(\to K\pi)\mu^+\mu^-$. These measurements found a 3.7σ deviation in the value of P_5', with 1 fb^{-1} luminosity in the $s \in [4.30, 8.68]$ GeV^2 bin [3]. Recently, this discrepancy was again seen at LHCb with a 3σ deviation with 3 fb^{-1} luminosity in two comparatively shorter adjacent bins $s \in [4,6]$ GeV^2 [4] and $s \in [6,8]$ GeV^2, which has also been confirmed by Belle in the larger bin $s \in [4,8]$ GeV^2 [6, 7]. Very recent results from the ATLAS [8] and CMS [9, 10] collaborations, presented at Moriond 2017, have also confirmed this discrepancy. Furthermore, LHCb also found a 2.6σ deviation in the value of $R_K = \mathrm{Br}(B \to K\mu^+\mu^-)/\mathrm{Br}(B \to Ke^+e^-)$ [12], and $\gtrsim 2\sigma$ in the $\mathrm{Br}(B_s \to \phi\mu^+\mu^-)$ [13]. Interestingly, all these deviations belong are in flavor changing neutral current (FCNC) transitions, $b \to s l^+ l^-$, where l^- denotes the final state leptons.

These anomalies have slowly piled up and received considerable attention in the literature (see for instance [11, 14]). It is also important to mention here that even the angular observables are form factor independent (FFI) but for precise theoretical predictions, one needs to

Received 24 January 2018, Revised 4 April 2018, Published online 11 May 2018

1) E-mail: ishtiaqmusab@gmail.com

2) E-mail: abdur.rehman@fuw.edu.pl

incorporate the factorizable and non-factorizable QCD corrections. The factorizable corrections are absorbed in the hadronic form factors while the non-factorizable corrections arise from hard scattering of the process and do not belong to the form factors. In this respect, there are some studies which focus on the question of whether these anomalies emerge from unknown factorizable power corrections or from NP [15, 16]. However, a global fit analysis with the present data strongly indicates that interpreting the mentioned anomalies as NP is a valid option [11]. In the present study, to determine the values of the angular observables, we have included both type of corrections up to next-to-leading order (NLO) and their expressions are given in Appendix B.

From the NP point of view, several extensions of the SM have been put forward [17–25]. Among these, the Z′ model is economical, due to the fact that besides the SM gauge group, it requires only one extra $U(1)'$ gauge symmetry associated with a neutral gauge boson, called Z′. The nature of the couplings of the Z′ boson with the quarks and leptons leads the FCNC transitions to the tree level. In this model, the NP effects come only through the short distance Wilson coefficients which are encapsulated in the new coefficients $C_9^{\rm tot} = C_9^{\rm SM} + C_9^{\rm Z'}$, $C_{10}^{\rm tot} = C_{10}^{\rm SM} + C_{10}^{\rm Z'}$, while the operator basis remains unchanged.

Several previous studies have shown a possible interpretation to alleviate the mismatch between the experimental data of different observables for the decay $\rm B \to K^*\mu^+\mu^-$ and their SM predictions in terms of the Z′ model [26–31] without any conflict. Therefore, it is natural to ask whether the Z′ model could explain the recently observed anomalies in the angular observables of the decay channel $\rm B \to K^*(\to K\pi)\mu^+\mu^-$. With this motivation, in the current study, we have analyzed the optimal observables $P_{1,2,3}$ and $P'_{4,5,6}$, in the low dimuon mass region, for $\rm B \to K^*(\to K\pi)\mu^+\mu^-$ in the SM and in the Z′ model. Besides these observables, we have also calculated the violation of lepton flavor universality (LFU) observables namely, $Q_{4(5)} = P'^{\mu}_{4(5)} - P'^{e}_{4(5)}$ [32]. For numerical calculations of these observables, we have used the LCSR values of the hadronic form factors [33], and for the Z′ parameters we have used the UTfit collaboration values, called $\mathcal{S}_1$, $\mathcal{S}_2$, and another different scenario, called $\mathcal{S}_3$, for which the numerical values are listed in Table A2.

We would like to mention here that the scenarios considered, labeled $\mathcal{S}_1$, $\mathcal{S}_2$ and $\mathcal{S}_3$, have the same coupling structure of the Z′ boson with the quarks and the leptons. However, the underlying difference between these scenarios is related to the different fit values of parameters such as a new weak phase and couplings of the Z′ model, for the decay process considered, available in the literature. For example, by using the all available experimental data on $\rm B_s$-$\bar{\rm B}_s$ mixing, the UTfit collaboration has found two solutions of a new weak phase, $\phi_{\rm sb}$, that arises due to the measurement ambiguities in the data; these are referred to $\mathcal{S}_1$ and $\mathcal{S}_2$. Similarly, another possible constraint on the parameters of the Z′ model is discussed in Ref. [49], which we label as $\mathcal{S}_3$.

This paper is organized as follows. Section 2.1 contains the effective Hamiltonian for the $\rm b \to sl^+l^-$ transition in the SM and in the Z′ model. The $\rm B \to K^*$ matrix elements in terms of form factors and the expression of the differential decay distribution are also given in this section. Formulae for the angular observables are given in Section 2.2. In Section 3, we plot the angular observables and their average values against dimuon mass s, and give a phenomenological analysis of these observables. In the last section we conclude our work. Appendix A contains the analytical expressions of the angular observables and the values of the input parameters. The contributions of factorizable and non-factorizable corrections at NLO are summarized in Appendix B.

2 Formulation for the analysis

2.1 Matrix elements and form factors

In the standard model, FCNC transitions $\rm b \to sl^+l^-$ occur at loop level, and their amplitude can be written as,

$$\begin{aligned}\mathcal{M}^{\rm SM}(\rm b\to sl^+l^-) =& -\frac{\alpha \rm G_F}{2\sqrt{2}\pi}\rm V_{tb}V_{ts}^*\\ \times&\Big\{\langle \rm K^*(p_{K^*},\epsilon)|\bar{s}\gamma^\mu Lb|B(p_B)\rangle (C_9^{\rm eff}\bar{\ell}\gamma^\mu\ell + C_{10}^{\rm SM}\bar{\ell}\gamma^\mu\gamma_5\ell)\\ &-2m_b C_7^{\rm eff}\langle \rm K^*(p_{K^*},\epsilon)|\bar{s}i\sigma_{\mu\nu}\frac{q^\nu}{q^2}Rb|B(p_B)\rangle\bar{\ell}\gamma^\mu\ell\Big\}, \end{aligned} \tag{1}$$

where $L,R = (1\mp\gamma^5)$, $p_{\rm K^*}$ and ϵ are the momentum and polarization of the K* meson, respectively, while $p_{\rm B}$ is the momentum of the B meson.

In the presence of Z′ the FCNC transitions could occur at tree level and the Hamiltonian can be written in the following form (see Refs. [34–37] for details):

$$\mathcal{H}_{\rm eff}^{Z'} = -\frac{4G_F}{\sqrt{2}}V_{\rm tb}V_{\rm ts}^*\Big[\Lambda_{\rm sb}C_9^{Z'}O_9 + \Lambda_{\rm sb}C_{10}^{Z'}O_{10}\Big], \tag{2}$$

$$\begin{aligned}\text{where, } \Lambda_{\rm sb} &= \frac{4\pi \rm e^{-i\phi_{sb}}}{\alpha_{em}V_{\rm tb}V_{\rm ts}^*}, C_9^{Z'} = |\mathcal{B}_{\rm sb}|S_{\ell\ell}^{LR},\\ \text{and}\quad C_{10}^{Z'} &= |\mathcal{B}_{\rm sb}|D_{\ell\ell}^{LR} \quad \text{with,}\\ \mathcal{S}_{\ell\ell}^{LR} &= \mathcal{B}_{\ell\ell}^{L} + \mathcal{B}_{\ell\ell}^{R}, \quad \mathcal{D}_{\ell\ell}^{LR} = \mathcal{B}_{\ell\ell}^{L} - \mathcal{B}_{\ell\ell}^{R}. \end{aligned} \tag{3}$$

$\mathcal{B}_{\rm sb}$ is the coupling of Z′ with quarks and $\mathcal{B}_{\ell\ell}^{L}$, $\mathcal{B}_{\ell\ell}^{R}$ are left and right-handed couplings of Z′ with leptons. One can notice from Eq. (3) that in the Z′ model, the operator basis remains the same as in the SM, while the Wilson

coefficients, C_9 and C_{10}, are modified. The total amplitude for the decay $\mathrm{B}\to\mathrm{K}^*\mathrm{l}^+\mathrm{l}^-$ is the sum of SM and Z' contributions, and can be written as follows,

$$\begin{aligned}\mathcal{M}^{\rm tot}(\mathrm{B}\to\mathrm{K}^*\mathrm{l}^+\mathrm{l}^-) \;=\; &-\frac{\alpha G_F}{2\sqrt{2}\pi}V_{\rm tb}V_{\rm ts}^*\Big\{\langle \mathrm{K}^*(p_{\mathrm{K}^*},\epsilon)|\bar{s}\gamma^\mu Lb|B(p_{\rm B})\rangle(C_9^{\rm tot}\bar{\ell}\gamma^\mu\ell+C_{10}^{\rm tot}\bar{\ell}\gamma^\mu\gamma_5\ell)\\ &-2m_b C_7^{\rm eff}\langle \mathrm{K}^*(p_{\mathrm{K}^*},\epsilon)|\bar{s}i\sigma_{\mu\nu}\frac{q^\nu}{q^2}Rb|B(p_{\rm B})\rangle\bar{\ell}\gamma^\mu\ell\Big\},\end{aligned} \tag{4}$$

where $C_9^{\rm tot}=C_9^{\rm eff}+\Lambda_{\rm sb}C_9^{Z'}$ and $C_{10}^{\rm tot}=C_{10}^{\rm SM}+\Lambda_{\rm sb}C_{10}^{Z'}$.

The matrix elements for the $B\to\mathrm{K}^*$ transition, which appear in Eq. (4), can be written in terms of form factors as follows:

$$\begin{aligned}\langle \mathrm{K}^*(p_{\mathrm{K}^*},\epsilon)|\bar{s}\gamma^\mu Lb|B(p_{\rm B})\rangle \;=\; &-\mathrm{i}q_\mu\frac{2m_{\mathrm{K}^*}}{s}\epsilon^*\cdot q\Big[A_3(s)-A_0(s)\Big]-\epsilon_{\mu\nu\lambda\sigma}\epsilon^{*\nu}p^\lambda_{\mathrm{K}^*}q^\sigma\frac{2V(s)}{(m_{\rm B}+m_{\mathrm{K}^*})}\\ &+\mathrm{i}\epsilon^*_\mu(m_{\rm B}+m_{\mathrm{K}^*})A_1(s)\mp\mathrm{i}(p_{\rm B}+p_{\mathrm{K}^*})_\mu\epsilon^*\cdot q\frac{A_2(s)}{(m_{\rm B}+m_{\mathrm{K}^*})},\end{aligned}$$

$$\begin{aligned}\langle \mathrm{K}^*(p_{\mathrm{K}^*},\epsilon)|\bar{s}i\sigma_{\mu\nu}q^\nu Rb|B(p_{\rm B})\rangle \;=\; &2\epsilon_{\mu\nu\lambda\sigma}\epsilon^{*\nu}p^\lambda_{\mathrm{K}^*}q^\sigma\;T_1(s)+i\epsilon^*\cdot q\Big\{q_\mu-\frac{(p_{\rm B}+p_{\mathrm{K}^*})_\mu s}{(m_{\rm B}^2-m_{\mathrm{K}^*}^2)}\Big\}T_3(s)\\ &+\mathrm{i}\Big\{\epsilon^*_\mu(m_{\rm B}^2-m_{\mathrm{K}^*}^2)-(p_{\rm B}+p_{\mathrm{K}^*})_\mu\epsilon^*\cdot q\Big\}\;T_2(s),\end{aligned} \tag{5}$$

where,

$$A_3(s) \;=\; \frac{m_{\rm B}+m_{\mathrm{K}^*}}{2m_{\mathrm{K}^*}}A_1(s)-\frac{m_{\rm B}-m_{\mathrm{K}^*}}{2m_{\mathrm{K}^*}}A_2(s). \tag{6}$$

Here $A_{0,1,2}(s)$, $V(s)$, $T_{1,2,3}(s)$ are the form factors and contain hadronic uncertainties. At leading order, by using the heavy quark limit, the QCD form factors follow the symmetry relations and can be expressed in terms of two universal form factors $\xi_\perp$ and $\xi_\parallel$ [38, 39].

$$\begin{aligned}\xi_\perp&=\frac{m_{\rm B}}{m_{\rm B}+m_{\mathrm{K}^*}}V,\\ \xi_\parallel&=\frac{m_{\rm B}+m_{\mathrm{K}^*}}{2E_{\mathrm{K}^*}}A_1-\frac{m_{\rm B}-m_{\mathrm{K}^*}}{m_{\rm B}}A_2.\end{aligned} \tag{7}$$

It is also important to mention here that the angular observables are soft form factor independent at LO in α_s (i.e., not totally dependent on FF). There is residual dependence which has been discussed, computed systematically and included in the predictions of the main papers of the field and even if, as expected, it does not play an important role, it induces a certain mild dependence on FF. In addition, for the s dependence of the universal form factors there are different parametrizations [5]. However, we have analyzed that the choice of parametrization is not so important at low s. In the current study, we use the following parametrization of the LCSR approach [33]:

$$\begin{aligned}V(s)&=\frac{r_1}{1-s/m_R^2}+\frac{r_2}{1-s/m_{fit}^2},\;\; A_1(s)=\frac{r_2}{1-s/m_{\rm fit}^2},\\ A_2(s)&=\frac{r_1}{1-s/m_{\rm fit}^2}+\frac{r_2}{(1-s/m_{\rm fit}^2)^2},\end{aligned} \tag{8}$$

where the parameters $r_{1,2}$, m_R^2 and $m_{\rm fit}^2$ are listed in Table 1. The uncertainty in the universal form factors $\xi_\perp$ and $\xi_\parallel$ arises from the uncertainty in the different parameters using in the LCSR approach, which is about 11% and 14%, respectively, as discussed in Ref. [38].

Table 1. The values of the fit parameters involved in the calculations of the form factors given in Eq. (8) [33].

	r_1	r_2	m_R^2/GeV^2	$m_{\rm fit}^2/\mathrm{GeV}^2$
$V(s)$	0.923	−0.511	28.30	49.40
$A_1(s)$		0.290		40.38
$A_2(s)$	−0.084	0.342		52.00

At NLO, the relations between the $T_i(s)$, where $i=1,2,3$, and the invariant amplitudes $\mathcal{T}_{\perp,\parallel}(s)$, where $\mathcal{T}_{\perp,\parallel}=\mathcal{T}^-_{\perp,\parallel}$, read as [40]:

$$T_1(s) \;=\; \mathcal{T}_\perp,\quad T_2(s)=\frac{2\mathcal{E}_{\mathrm{K}^*}}{m_{\rm B}}\mathcal{T}_\perp,\quad T_3(s)=\mathcal{T}_\perp+\mathcal{T}_\parallel, \tag{9}$$

where $\mathcal{E}_{\mathrm{K}^*}=(m_{\rm B}^2+m_{\mathrm{K}^*}^2-s)/2m_{\rm B}$ is the energy of the kaon in the rest frame of the B-meson and $\mathcal{T}_{\perp,\parallel}(s)$ are defined in Eq. (B4) of Appendix B.

The four-fold differential decay distribution for the cascade decay $\mathrm{B}\to\mathrm{K}^*(\to\mathrm{K}\pi)\mathrm{l}^+\mathrm{l}^-$ is completely described by the four independent kinematic variables. These are the three angles: θ_{K^*} is the angle between the K and B mesons in the rest frame of K^*, θ_ℓ is the angle between the lepton and B meson in the dilepton rest frame, and ϕ is the azimuthal angle between the dilepton rest frame and the K^* rest frame; and the fourth variable is the dilepton invariant squared mass s. The explicit dependence of the differential decay distribution on these kinematic variables can be expressed as follows:

$$\frac{\mathrm{d}^4\Gamma}{\mathrm{d}s\mathrm{d}\cos\theta_\ell\mathrm{d}\cos\theta_{\mathrm{K}^*}\mathrm{d}\phi}=\frac{9}{32\pi}\widetilde{\Gamma}(s,\theta_\ell,\theta_{\mathrm{K}^*},\phi), \tag{10}$$

where

$$\begin{aligned}&\widetilde{\Gamma}(s,\theta_\ell,\theta_{\rm K^*},\phi)=\\&J_1^s\sin^2\theta_{\rm K^*}+J_1^c\cos^2\theta_{\rm K^*}+\left(J_2^s\sin^2\theta_{\rm K^*}+J_2^c\cos^2\theta_{\rm K^*}\right)\cos2\theta_\ell\\&+J_3\sin^2\theta_{\rm K^*}\sin^2\theta_\ell\cos2\phi+J_4\sin2\theta_{\rm K^*}\sin2\theta_\ell\cos\phi\\&+J_5\sin2\theta_{\rm K^*}\sin\theta_\ell\cos\phi+(J_6^s\sin^2\theta_{\rm K^*}+J_6^c\cos^2\theta_{\rm K^*})\cos\theta_\ell\\&+J_7\sin2\theta_{\rm K^*}\sin\theta_\ell\sin\phi+J_8\sin2\theta_{\rm K^*}\sin2\theta_\ell\sin\phi\\&+J_9\sin^2\theta_{\rm K^*}\sin^2\theta_\ell\sin2\phi.\end{aligned}\tag{11}$$

The full physical region phase space of kinematic variables is given by

$$\begin{aligned}&4m_\ell^2\leqslant s\leqslant(m_{\rm B}-m_{\rm K^*})^2,\qquad 0\leqslant\theta_\ell\leqslant\pi,\\&0\leqslant\theta_{\rm K^*}\leqslant\pi,\qquad 0\leqslant\phi\leqslant2\pi,\end{aligned}\tag{12}$$

where $m_{\rm B}$, $m_{\rm K^*}$, m_ℓ are the masses of the B meson, $\rm K^*$ meson and lepton, respectively.

The expressions of coefficients $J_i^{(a)}=J_i^{(a)}(s)$ for $i=1,....,9$ and $a=s,c$ as a function of the dilepton mass s, are given in Appendix A in Eq. (A1). As we do not consider the scalar contribution in this study, $J_6^c=0$.

2.2 Expressions of the angular observables

The definitions of the FFI angular observables (optimal observables) are given in Ref. [14],

$$\begin{aligned}P_1(s)&=\frac{J_3}{2J_2^s},\quad P_2(s)=\beta_\ell\frac{J_6^s}{8J_2^s},\quad P_3(s)=-\frac{J_9}{4J_2^s},\\P_4(s)&=\frac{\sqrt{2}J_4}{\sqrt{-J_2^c(2J_2^s-J_3)}},P_5(s)=\frac{\beta_\ell J_5}{\sqrt{-2J_2^c(2J_2^s+J_3)}},\\P_6(s)&=-\frac{\beta_\ell J_7}{\sqrt{-2J_2^c(2J_2^s-J_3)}}.\end{aligned}\tag{13}$$

The primed observables (related to the P_i $(i=4,5,6)$) which are simpler and more efficient to fit experimentally, are defined as,

$$\begin{aligned}P_4'&\equiv P_4\sqrt{1-P_1}=\frac{J_4}{\sqrt{-J_2^cJ_2^s}},\\P_5'&\equiv P_5\sqrt{1+P_1}=\frac{J_5}{2\sqrt{-J_2^cJ_2^s}},\\P_6'&\equiv P_6\sqrt{1-P_1}=\frac{-J_7}{2\sqrt{-J_2^cJ_2^s}}.\end{aligned}\tag{14}$$

3 Results and discussion

In this section, we will present the numerical analysis of the angular observables. All of the numerical results are taken from a Mathematica code written by the authors. Before the analysis, we would like to write the different definitions of angular observables that are set by LHCb [4] and used theoretically in the literature,

$$\begin{aligned}P_2^{\rm exp}&=-P_2,\quad P_3^{\rm exp}=-P_3,\quad P_4'^{\rm exp}=-\frac{1}{2}P_4',\\P_6'^{\rm exp}&=-P_6',\quad P_1^{\rm exp}=P_1,\quad P_5'^{\rm exp}=P_5'.\end{aligned}\tag{15}$$

For the numerical analysis, the values of LCSR form factors and relevant fit parameters are listed in Table 1. The values of Wilson coefficients and other input parameters are listed in Appendix A in Tables A1 and A3, respectively. Regarding the coupling parameters of Z′ with quarks and leptons, there are some severe constraints from different inclusive and exclusive B- meson channels [42], particularly from the two different fitting values for $\rm B_s-\bar{B}_s$ mixing data by the UTFit collaboration[43]. In this study, these are the two fitting values $\mathcal{S}_1$ and $\mathcal{S}_2$ and their numerical values are listed in Table A2. The other scenario we consider, denoted by $\mathcal{S}_3$, is obtained from the analysis of $\rm B\to X_s\mu^+\mu^-$ [45], $\rm B\to K^*\mu^+\mu^-$ [46, 47] and $\rm B\to\mu^+\mu^-$ [48]. The numerical values of scenario $\mathcal{S}_3$ are chosen from Refs. [44, 49] and also listed in Table A2. The purpose of the following analysis is to check that these constrained Z′ parameters could accomodate the anomalies in the angular observables, particularly in P_5'.

3.1 P-observables in different bin sizes

The numerical values of angular observables in different low s bins in SM and in $\mathcal{S}_1$, $\mathcal{S}_2$ and $\mathcal{S}_3$ are given in Table 2. For comparison with experimental measurements, the maximum likelihood fit results of LHCb [4] are also given in the table. The ranges in the values of angular observables in $\mathcal{S}_1$, $\mathcal{S}_2$ and $\mathcal{S}_3$ are found by setting the upper and lower values of parametric space of these scenarios. These results are also shown graphically in Figs. 1 and 2, where the black crosses are the data points taken from the last column of Table 2 and the black dashed lines correspond to the SM, while the green, red and blue bands correspond to the $\mathcal{S}_1$, $\mathcal{S}_2$ and $\mathcal{S}_3$ scenarios of the Z′ model, respectively. The upper curve of the band corresponds to the upper values of parametric space while the lower curve of the band corresponds to the lower values of parametric space of the scenario. In our different bin size analysis, we have not included the preliminary results from Belle [6, 7], ATLAS [8] and CMS*[9, 10] because their bin intervals are different from those of LHCb [4], as we have discussed in this section. In Fig. 1, the gray shaded region corresponds to the uncertainty in the SM values due to the uncertainty in different input parameters. One can see from the left-hand panels of Figs. 1 and 2 that the uncertainty band in the SM does not preclude the effects of the Z′ model. Therefore, we have not provided the SM uncertainty in Table 2 and hence in the right-hand panels of Figs. 1 and 2[1)].

1) See Fig. 6 of Ref. [11] for a recent analysis with these new results.

Table 2. Results for $\langle P\rangle$-observables and their comparison with maximum likelihood fit results of Ref. [4] for different bin sizes.

Obs.	SM prediction	$\mathcal{S}_1$	$\mathcal{S}_2$	$\mathcal{S}_3$	measurement [4]
$0.1<s<0.98$ GeV^2					
$\langle P_1\rangle$	-0.002	$-0.002\leftrightarrow-0.008$	$-0.002\leftrightarrow-0.002$	$-0.002\leftrightarrow-0.009$	$-0.099^{+0.168}_{-0.163}\pm0.014$
$\langle P_2\rangle$	-0.106	$-0.134\leftrightarrow-0.113$	$-0.116\leftrightarrow-0.102$	$0.042\leftrightarrow-0.059$	$-0.003^{+0.051}_{-0.052}\pm0.007$
$\langle P_3\rangle$	-0.0001	$0.000\leftrightarrow-0.0002$	$-0.000\leftrightarrow-0.001$	$-0.000\leftrightarrow-0.0001$	$0.113^{+0.079}_{-0.079}\pm0.006$
$\langle P_4'\rangle$	0.267	$0.175\leftrightarrow0.155$	$0.230\leftrightarrow0.171$	$0.405\leftrightarrow0.380$	$0.185^{+0.158}_{-0.154}\pm0.023$
$\langle P_5'\rangle$	0.740	$0.747\leftrightarrow0.473$	$0.712\leftrightarrow0.497$	$-0.209\leftrightarrow0.424$	$0.387^{+0.132}_{-0.133}\pm0.052$
$\langle P_6'\rangle$	-0.158	$-0.447\leftrightarrow-0.585$	$-0.384\leftrightarrow-0.566$	$0.466\leftrightarrow0.400$	$0.034^{+0.134}_{-0.135}\pm0.015$
$1.1<s<2.5$ GeV^2					
$\langle P_1\rangle$	-0.007	$-0.008\leftrightarrow-0.008$	$-0.007\leftrightarrow-0.008$	$-0.006\leftrightarrow-0.006$	$-0.415^{+0.519}_{-0.636}\pm0.038$
$\langle P_2\rangle$	-0.433	$-0.417\leftrightarrow-0.161$	$-0.406\leftrightarrow-0.187$	$0.097\leftrightarrow-0.347$	$-0.373^{+0.146}_{-0.199}\pm0.027$
$\langle P_3\rangle$	0.0001	$-0.000\leftrightarrow0.001$	$0.000\leftrightarrow0.001$	$0.001\leftrightarrow0.001$	$0.350^{+0.330}_{-0.254}\pm0.015$
$\langle P_4'\rangle$	0.023	$-0.113\leftrightarrow-0.173$	$-0.040\leftrightarrow-0.13$	$0.170\leftrightarrow0.200$	$-0.163^{+0.232}_{-0.240}\pm0.021$
$\langle P_5'\rangle$	0.225	$0.275\leftrightarrow-0.208$	$0.211\leftrightarrow-0.141$	$0.249\leftrightarrow0.160$	$0.289^{+0.220}_{-0.202}\pm0.023$
$\langle P_6'\rangle$	-0.078	$-0.432\leftrightarrow-0.533$	$-0.400\leftrightarrow-0.536$	$0.689\leftrightarrow0.520$	$-0.463^{+0.202}_{-0.221}\pm0.012$
$2.5<s<4.0$ GeV^2					
$\langle P_1\rangle$	-0.023	$-0.025\leftrightarrow-0.026$	$-0.024\leftrightarrow-0.025$	$-0.032\leftrightarrow-0.024$	$0.571^{+2.404}_{-1.714}\pm0.045$
$\langle P_2\rangle$	-0.228	$-0.215\leftrightarrow0.154$	$-0.188\leftrightarrow0.110$	$-0.341\leftrightarrow-0.280$	$-0.636^{+0.444}_{-1.735}\pm0.015$
$\langle P_3\rangle$	0.001	$-0.000\leftrightarrow0.002$	$0.001\leftrightarrow0.002$	$0.004\leftrightarrow0.004$	$0.745^{+2.587}_{-0.861}\pm0.030$
$\langle P_4'\rangle$	-0.282	$-0.355\leftrightarrow-0.394$	$-0.320\leftrightarrow-0.371$	$-0.314\leftrightarrow-0.205$	$-0.713^{+0.410}_{-1.305}\pm0.024$
$\langle P_5'\rangle$	-0.400	$-0.204\leftrightarrow-0.667$	$-0.339\leftrightarrow-0.628$	$0.722\leftrightarrow-0.294$	$-0.066^{+0.343}_{-0.364}\pm0.023$
$\langle P_6'\rangle$	-0.066	$-0.313\leftrightarrow-0.350$	$-0.309\leftrightarrow-0.372$	$0.568\leftrightarrow0.508$	$0.205^{+0.962}_{-0.341}\pm0.013$
$4.0<s<6.0$ GeV^2					
$\langle P_1\rangle$	-0.055	$-0.053\leftrightarrow-0.053$	$-0.054\leftrightarrow-0.053$	$-0.064\leftrightarrow-0.062$	$0.180^{+0.364}_{-0.348}\pm0.0.027$
$\langle P_2\rangle$	0.206	$0.088\leftrightarrow0.357$	$0.170\leftrightarrow0.341$	$-0.407\leftrightarrow0.146$	$0.042^{+0.088}_{-0.087}\pm0.011$
$\langle P_3\rangle$	0.001	$-0.000\leftrightarrow0.003$	$0.000\leftrightarrow0.003$	$0.003\leftrightarrow0.004$	$0.083^{+0.187}_{-0.184}\pm0.023$
$\langle P_4'\rangle$	-0.443	$-0.460\leftrightarrow-0.472$	$-0.452\leftrightarrow-0.465$	$-0.477\leftrightarrow-0.446$	$-0.448^{+0.169}_{-0.172}\pm0.020$
$\langle P_5'\rangle$	-0.761	$-0.492\leftrightarrow-0.837$	$-0.653\leftrightarrow-0.829$	$0.682\leftrightarrow-0.514$	$-0.300^{+0.158}_{-0.159}\pm0.023$
$\langle P_6'\rangle$	-0.036	$-0.182\leftrightarrow-0.198$	$-0.178\leftrightarrow-0.214$	$0.249\leftrightarrow0.268$	$-0.032^{+0.167}_{-0.166}\pm0.007$

The plots in the first and third rows of Fig. 1 represent the variation in the values of $P_{1,3}$ and their average values $\langle P_{1,3}\rangle$ as a function of s in the SM and in the different scenarios of the Z$'$ model. From these plots one can see that the values of these observables are quite small in the SM and not much enhanced when we incorporate the Z$'$ effects. One can also see from Fig. 1 that the SM values of $\langle P_1\rangle$ lie inside the measured values. As the error in the measurement is huge, no significant result can be drawn from this observable with the current data. On the other hand the values of $\langle P_3\rangle$ in the last two bins are within the measured values, while in the first two bins the SM values are outside the error bars. However, to say something about any discrepancy in these observables, reduction in the experimental uncertainties is required.

The plots in the second row of Fig. 1 show the variation in the values of P_2 and its average $\langle P_2\rangle$ against dilepton mass s. It can be seen from these figures that the values of these observables are significantly influenced by the presence of Z$'$ effects. The right-hand plot in the second row of Fig. 1 shows that the SM values of $\langle P_2\rangle$ in the bins $s\in[1.1,2.5]$ and $s\in[2.5,4.0]$ lie within the measurements and also in the bin $s\in[4.0,6,0]$ when the theoretical uncertainties of the input parameters are taken into account. However, in the first bin $s\in[0.1,0.98]$, the SM value of $\langle P_2\rangle$ looks mismatched from the experimental value. It is worth mentioning here, though, that the measurement performed by LHCb in this bin does not include the $m_\ell-$ suppressed terms which are important in the very low s region, and it was found in Ref. [41] that the impact of these terms is about a 23% reduction in the value of $\langle P_2\rangle$. Regarding this, it is mentioned in Ref. [15] that in the first bin, LHCb actually measured $\langle\hat{P}_2\rangle$ instead of $\langle P_2\rangle$. Therefore, in principle, one could say that, to date, there is no mismatch between the SM predicted values of $\langle P_2\rangle$ and the experimental values.

In the first row of Fig. 2, we have displayed P_4' and its average value, $\langle P_4'\rangle$, in the SM and in the different scenarios of the Z$'$ model, as a function of s. One can see from these plots that the Z$'$ effects are quite significant in the P_4' values in the low s region but mild at larger values of s. However, the SM values of $\langle\mathcal{P}_4'\rangle$ in all four bins lie inside the measured values.

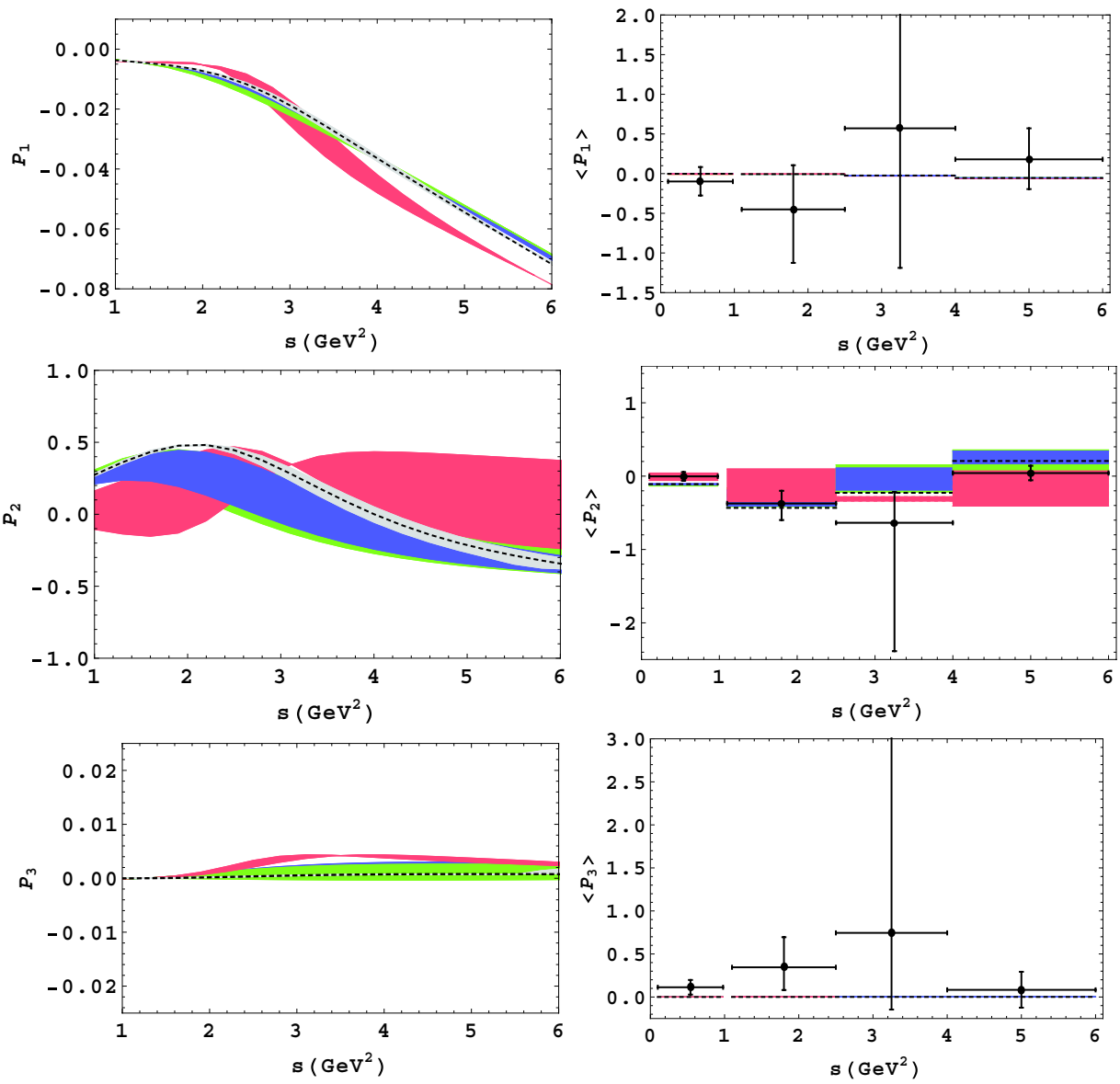

Fig. 1. (color online) The dependence of the optimal observables for the decay $B \to K^*(\to K\pi)l^+l^-$, $P_{1,2,3}$ and $\langle P_{1,2,3}\rangle$, on s. The black dashed lines correspond to the SM while the green, blue and red bands correspond to the $\mathcal{S}_1$, $\mathcal{S}_2$ and $\mathcal{S}_3$ scenarios of the Z′ model, respectively.

The results of P_5' and it's average value $\langle P_5'\rangle$ in the SM and in the Z′ models are presented in the second row of Fig. 2. The values are significantly changed from the SM values when we incorporate the Z′ effects. It can be noticed in the bin $s=4$ to 6 GeV^2 that the SM average value $\langle P_5'\rangle$ does not match the experimental values, and as mentioned in the Introduction, LHCb found a 3σ deviation in this bin. It can be seen from the figure that this discrepancy can be alleviated by the $\mathcal{S}_3$ (red band) of the Z′ model. On the other hand, for the UTfit scenarios, namely, $\mathcal{S}_1$ and $\mathcal{S}_2$, when we take the upper and lower limit values of the current parametric space of these scenarios (green and blue bands), the P_5' anomaly in the bin $s\in[4,6]$GeV^2 cannot be accommodated. However, if the values of different parameters are chosen randomly within the allowed range, then one could accommodate the P_5' anomaly in this bin by $\mathcal{S}_1$ but not with $\mathcal{S}_2$. Therefore, it seems that the $\mathcal{S}_2$ of UTfit is not consistent with the present data, while the parametric space of $\mathcal{S}_1$, the left (right) couplings, $(B^L_{\ell\ell},\ B^R_{\ell\ell})$, of Z′ with leptons is severely constrained, as shown in Fig. 3.

In the third row of Fig. 2, we show the variation of P_6' and $\langle P_6'\rangle$ as a function of s. Similar to $P_{1,3}$, the SM value of this observable is also suppressed. The SM value of P_6' is consistent with the data with large error bars, but there is a 2σ deviation in one bin $s\in[1.1,2.5]$, which

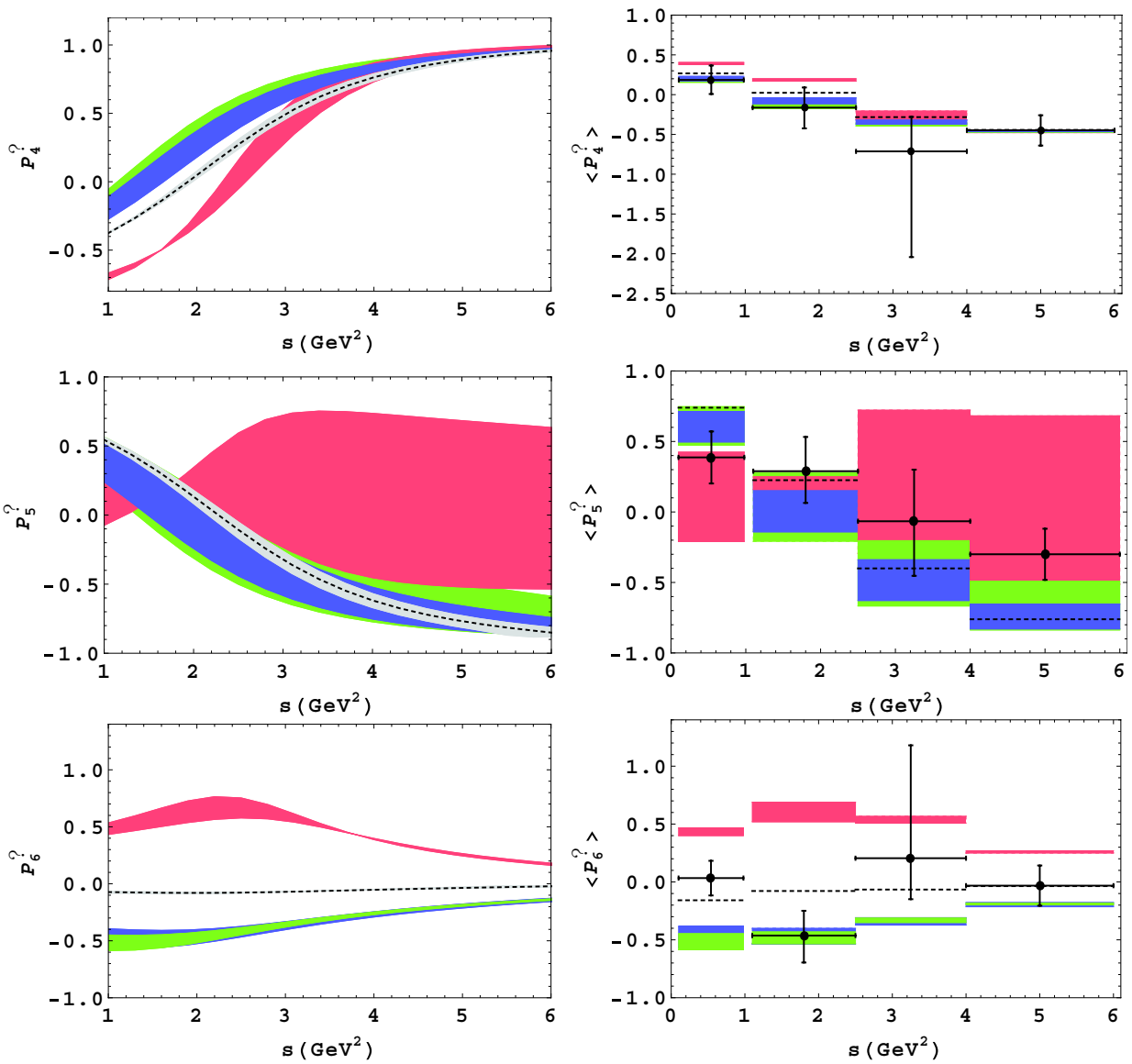

Fig. 2. (color online) The dependence of the optimal observables for the decay $B \to K^*(\to K\pi)l^+l^-$, $P'_{4,5,6}$ and $\langle P'_{4,5,6}\rangle$, on s. The black dashed lines correspond to the SM while the green, blue and red bands correspond to the $\mathcal{S}_1$, $\mathcal{S}_2$ and $\mathcal{S}_3$ scenarios of the Z′ model, respectively.

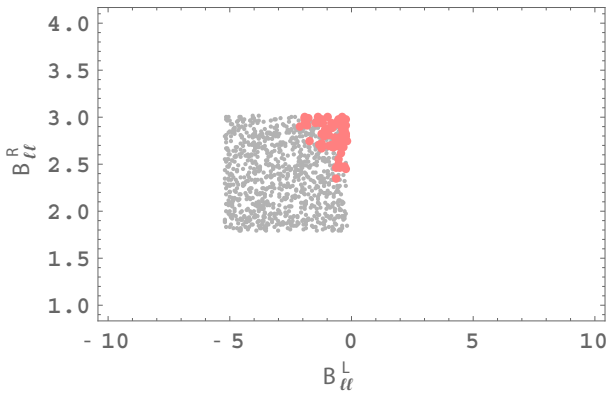

Fig. 3. (color online) The gray dots represent the left (right) couplings, ($B^L_{\ell\ell}$, $B^R_{\ell\ell}$), of Z′ with leptons in $\mathcal{S}_1$, while the red dots show the values of these couplings after accommodating the P'_5 anomaly in $s\in[4.0,6.0]$ GeV^2.

Table 3. Results for $\langle P\rangle$-observables for $s\in[1.0,6.0]$ GeV^2 and their comparison with LHCb maximum likelihood fit results of Ref. [4] in different bin sizes and Belle results [6, 7].

Obs.	SM prediction	$\mathcal{S}_1$	$\mathcal{S}_2$	$\mathcal{S}_3$	measurement
$\langle P_1\rangle$	-0.033±0.001	$-0.032\leftrightarrow-0.034$	$-0.033\leftrightarrow-0.033$	$-0.039\leftrightarrow-0.036$	$0.080^{+0.248}_{-0.245}\pm0.044$ [4]
$\langle P_2\rangle$	0.091±0.033	$0.133\leftrightarrow-0.162$	$0.087\leftrightarrow-0.135$	$0.254\leftrightarrow0.106$	$-0.162^{+0.072}_{-0.073}\pm0.010$ [4]
$\langle P_3\rangle$	0.001±0.000	$-0.000\leftrightarrow0.002$	$0.000\leftrightarrow0.002$	$0.003\leftrightarrow0.003$	$0.205^{+0.135}_{-0.134}\pm0.017$ [4]
$\langle P_4'\rangle$	−0.264±0.014	$-0.333\leftrightarrow-0.368$	$-0.298\leftrightarrow-0.347$	$-0.195\leftrightarrow-0.256$	$-0.336^{+0.124}_{-0.122}\pm0.12$ [4] $-0.095^{+0.302}_{-0.309}\pm0.174$ [6] $-0.22^{+0.35}_{-0.34}\pm0.15$ [7]
$\langle P_5'\rangle$	−0.378±0.051	$-0.197\leftrightarrow-0.617$	$-0.322\leftrightarrow-0.583$	$0.572\leftrightarrow-0.260$	$-0.049^{+0.107}_{-0.108}\pm0.014$ [4] $0.385^{+0.276}_{-0.285}\pm0.099$ [6] $0.43^{+0.26}_{-0.28}\pm0.10$ [7]
$\langle P_6'\rangle$	−0.056±−0.000	$-0.287\leftrightarrow-0.330$	$-0.276\leftrightarrow-0.345$	$0.452\leftrightarrow0.403$	$-0.166^{+0.108}_{-0.108}\pm0.021$ [4] $-0.202^{+0.278}_{-0.270}\pm0.172$ [6]

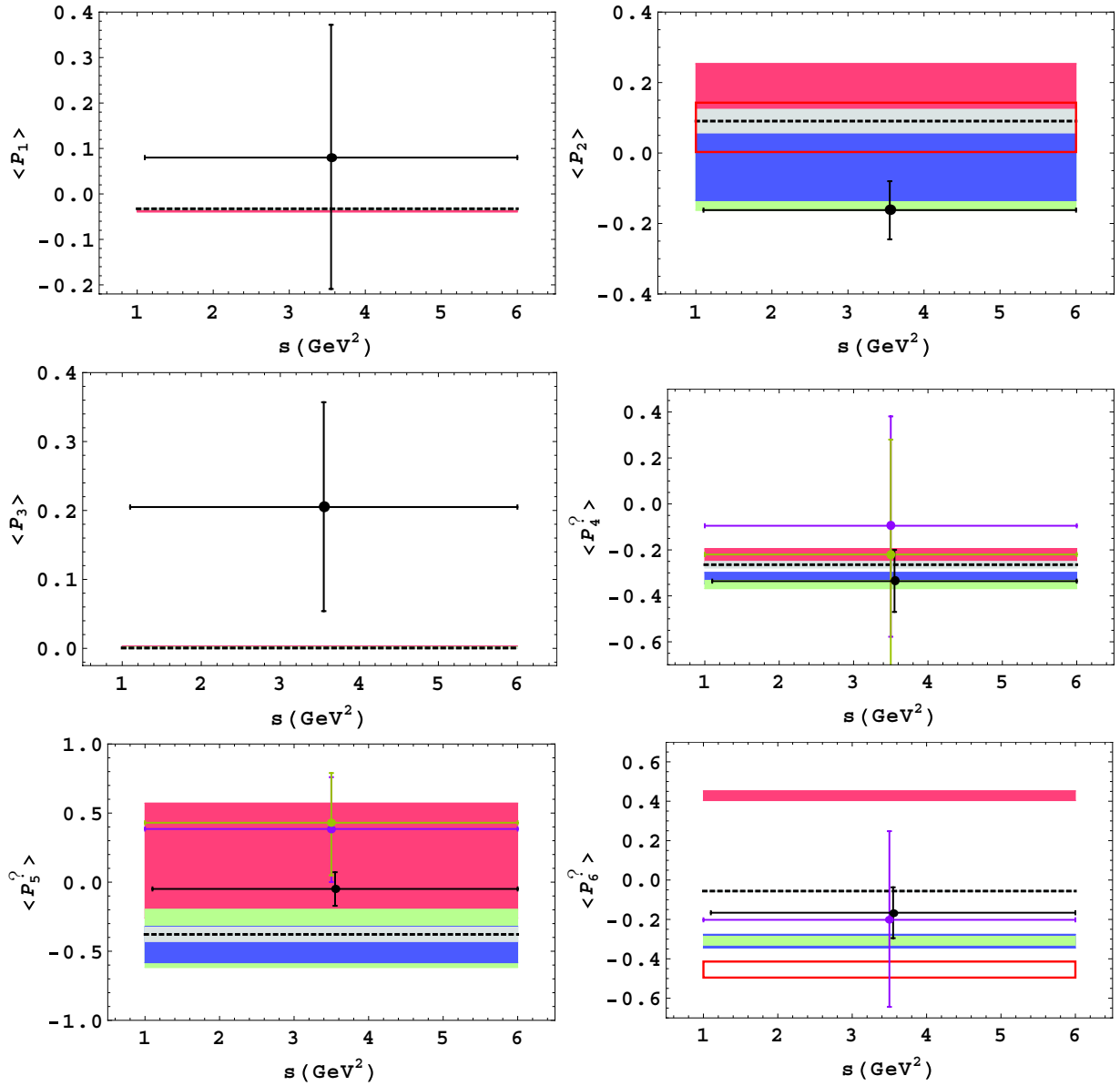

Fig. 4. (color online) Optimal observables for $s\in[1.0,6.0]$ GeV^2, where magenta [6] and yellow [7] error bars correspond to Belle measurements available for some of these observables. The empty red box in $\langle P_2\rangle$ and $\langle P_6'\rangle$ represents the $\mathcal{S}_3$ when we choose $\phi_{\rm sb}=-150\pm10$, given in Table A2 of Appendix A. The black dashed lines correspond to the SM while the green, blue and red bands correspond to the $\mathcal{S}_1$, $\mathcal{S}_2$ and $\mathcal{S}_3$ scenarios of the Z′ model, respectively.

will probably disappear when more data is available. One can also notice that in contrast to the $P_{1,3}$, the value of P_6' is significantly enhanced in the Z′ model. It is also noticed that in the Z′ model the value of P_6' is positive in scenarios $\mathcal{S}_1$ and $\mathcal{S}_2$ while it becomes negative in $\mathcal{S}_3$. As for the present analysis in $\mathcal{S}_3$, we set the value of $\phi_{\rm sb}=150\pm10$. In contrast to this, if we choose $\phi_{\rm sb}=-150\pm10$, which is also allowed (see Table 5), then this negative value becomes positive.

3.2 *P*-observables in $s\in[1.0,6.0]$ GeV^2

Besides the analysis of angular observables in shorter bins at low s region (discussed in the previous section), we have also analyzed these observables in the full $s\in[1.0,6.0]$ GeV^2 region. The results for P-observables in $s\in[1.0,6.0]$ GeV^2 are summarized in Table 3 and the corresponding plots are shown in Fig. 4. In this figure, black error bar corresponds to the LHCb result [4], while magenta and yellow error bars correspond to the Belle measurements for some of these observables [6, 7]. However, the LHCb results are in the bin $s\in[1.1,6.0]$ GeV^2, while the Belle measurements [6, 7] are in $s\in[1.0,6.0]$ GeV^2. In addition, recently the ATLAS collaboration announced its results for $s\in[0.04,6.0]$ GeV^2 [8], which is not included in the current analysis. The empty red boxes in the plots of $\langle P_2\rangle$ and $\langle P_6'\rangle$ represent the $\mathcal{S}_3$ scenario when we choose $\phi_{\rm sb}=-150\pm10$.

From Fig. 4, the values of $\langle P_1\rangle$ and $\langle P_4'\rangle$ in the SM and in all the three scenarios of Z′ lie within the current measurements. However, the error bars are huge. Therefore, to extract any information about NP requires precise measurements of these observables. It is also noticed that the values of $\langle P_1\rangle$ in the SM and in the Z′ scenarios are very close. Consequently, this observable, even after the reduction of error bars, is not a good candidate to constrain the Z′ parameter space. On the other hand, $\langle P_4'\rangle$ could be helpful to constrain the Z′ parameter space, if any mismatch appears in future in the bin [1, 6] GeV^2. The SM value of $\langle P_3\rangle$ is small and is not enhanced in the Z′ model. However, the measured value is well above the SM prediction, with huge error bars, and more precision is needed to draw any conclusion from this observable. From the plot of $\langle P_2\rangle$ in Fig. 4, one can deduce that the SM value of $\langle P_2\rangle$ does not lie within the measured value of LHCb. However, the values of $\langle P_2\rangle$ in $\mathcal{S}_1$ and $\mathcal{S}_2$ are within the measurements while in $\mathcal{S}_3$, the value is outside the measured error bars. For $\langle P_6'\rangle$, we have two different measurements, as shown in the plot and, different to $\langle P_2\rangle$, the value of $\langle P_6'\rangle$ lies within these measurements. However, similar to $\langle P_2\rangle$, the values of $\langle P_6'\rangle$ in $\mathcal{S}_1$ and $\mathcal{S}_2$ lie within the measurements while the value in $\mathcal{S}_3$ lies outside the measured values (see red bands in both plots). Regarding $\mathcal{S}_3$, it is interesting to check whether the values of $\langle P_2\rangle$ and $\langle P_6'\rangle$ could be reduced to current measurements. For this purpose, we choose the weak phase with opposite sign i.e., $\phi_{\rm sb}=-150\pm10$ (see Table A2 in Appendix A) and represent them in plots by empty red boxes. In Fig. 4, by looking at the empty red box in the $\langle P_2\rangle$ plot, the value is reduced but still well above the current measurement. In contrast, the value of $\langle P_6'\rangle$ reduces to the Belle measurements [6]. However, more statistics on the observables $\langle P_2\rangle$ and $\langle P_6'\rangle$ would be helpful to constrain the Z′ parameters, particularly the sign and the magnitude of the new weak phase $\phi_{\rm sb}$.

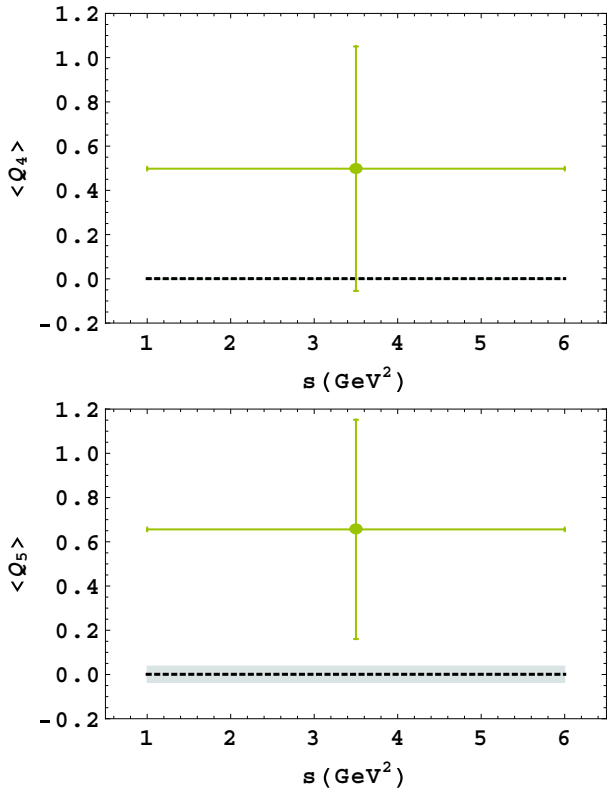

Fig. 5. (color online) Optimal observables Q_4, Q_5 for $s\in[1.00,6.00]$ GeV^2, where the yellow error bars correspond to recent Belle measurements [7]. The black dashed lines correspond to the SM.

For the $\langle P_5'\rangle$ plots of Fig. 3, the values in the SM and in $\mathcal{S}_1$, $\mathcal{S}_2$ lie outside the error bars of the experimental data points, while the values in the $\mathcal{S}_3$ model are well inside the all data points. In general, from the plots of Fig. 3, one concludes that the considered models do have potential to remove the mismatch between theory and experiment, but it is not conclusive at present. We hope more precise measurements will clear the situation.

3.3 $Q_{4,5}$ for $s\in[1.0,6.0]$ GeV^2

In Fig. 5, we have plotted the lepton flavor universality violation (LFUV) observables $\langle Q_{4(5)}\rangle$ against s. The values are quite small in the SM, approximately $\langle Q_{4(5)}\rangle = 8.8\pm2.1\times10^{-3}(7.5\pm3.6\times10^{-3})$ in the bin

$s \in [1,6]\text{GeV}^2$. We have also found that the effects of Z′ are negligible. This is trivial, since Eq. (3) implies $C_{9,10}^{\mathrm{Z}',\mu} = C_{9,10}^{\mathrm{Z}',e}$. However, the error bars are quite large and need more experimental data to find accurate values of these observables.

4 Conclusion

In this study, we have calculated the angular observables P_i and their average values $\langle P_i \rangle$ in the SM and in the non-universal family of Z′ models for the decay channel $\mathrm{B} \to \mathrm{K}^*(\to \mathrm{K}\pi)\mathrm{l}^+\mathrm{l}^-$. The expressions of the angular observables are given in the form of coefficient $J_i(s)$ which are written in terms of auxiliary functions $g_i(h_i)$ in Eq. (A1). As in the literature, these $J_i(s)$ coefficients, in general, are expressed via transversity amplitudes, $A_\perp$, $A_\parallel$ and A_0, so the relations of these transversity amplitudes with auxiliary function $g_i(h_i)$ are also given in Eq. (A4). To see the Z′ effects on these observables, we have used the UTfit collaboration constraints for the Z′ parameters, called scenarios $\mathcal{S}_1$ and $\mathcal{S}_2$. Besides, we have also considered another scenario, called $\mathcal{S}_3$. From the present analysis, in all three scenarios of Z′ for small values of s, i.e. the large recoil region, the values of angular observables are significantly changed from their SM values. The current analysis shows that, apart from the scenario $\mathcal{S}_1$, the scenarios $\mathcal{S}_2$ and $\mathcal{S}_3$ of Z′ model have potential to accommodate the mismatch between the recent experimental measurements and the SM values of some of the angular observables in some bins of s. For instance, there is a discrepancy between the experimentally measured value and SM value of P_5' in the region $s \in [4,6]$ GeV^2. In the current study it has been found that the scenario $\mathcal{S}_3$ of Z′ could adjust this mismatched value to the measured value in this bin. On the other hand, this mismatch cannot be accommodated on taking the maximum and minimum values of different parameters of scenarios $\mathcal{S}_1$ and $\mathcal{S}_2$ of the UTfit collaboration. However, when we choose random values of different parameters in the allowed region of these scenarios, one can accommodate the P_5' anomaly with scenario $\mathcal{S}_2$ but not with scenario $\mathcal{S}_1$. It is also noticed that the P_5' anomaly further constrains the allowed parameter space of $\mathcal{S}_2$. Furthermore, we have also calculated the angular observables $\langle P_i \rangle$ and the LFUV observables $\langle Q_{4,5} \rangle$ in the large bin $s \in [1,6]$ and plotted with the measured data. However, the error bars are quite large in this bin and more statistics are needed to draw any conclusions. The CMS and ATLAS collaborations recently announced preliminary results on angular observables at Moriond 2017, which still show the tension between experimental measurements and the SM predictions. Therefore, in general, as available data increases and the statistical errors are reduced, these observables should be quite promising to say something about the constraints on the coupling of the Z′ boson with the quarks and leptons, and consequently about the status of the Z′ model.

Appendix A

The expressions for J_i which appear in Eqs. (13) and (14) are as follows:

$$
\begin{aligned}
J_1^s &= \frac{3s\beta_l^2}{2}\Big[p_{\mathrm{K}^*}^2 s\big(|g_1|^2+|h_1|^2\big)+|g_2|^2+|h_2|^2\Big] \\
&\quad +\frac{8m_l^2}{s}(p_{\mathrm{K}^*}^2 s|h_1|^2+|h_2|^2), \\
J_1^c &= \frac{2}{m_{\mathrm{K}^*}^2}\Big[32\mathrm{a}_0^2 C_{10}^{\mathrm{tot}^2} m_{\mathrm{K}^*}^2 m_l^2 p_{\mathrm{K}^*}^2+\beta_l^2 s|E_{\mathrm{K}^*} g_2 \\
&\quad +2\sqrt{s}p_{\mathrm{K}^*}^2 g_3|^2+\big(2-\beta_l^2\big)s|E_{\mathrm{K}^*} h_2+2\sqrt{s}p_{\mathrm{K}^*}^2 h_3|^2\Big], \\
J_2^s &= \frac{1}{2}s\beta_l^2\Big[P_{\mathrm{K}^*}^2 s\big(|g_1|^2+|h_1|^2\big)+|g_2|^2+|h_2|^2\Big], \\
J_2^c &= -\frac{2\beta_l^2 s}{m_{\mathrm{K}^*}^2}\Big[|E_{\mathrm{K}^*}\mathrm{g}_2+2\sqrt{s}p_{\mathrm{K}^*}^2 g_3|^2+|E_{\mathrm{K}^*} h_2 \\
&\quad +2\sqrt{s}p_{\mathrm{K}^*}^2 h_3|^2\Big], \\
J_3 &= s\beta_l^2\Big[p_{\mathrm{K}^*}^2 s\big(|g_1|^2+|h_1|^2\big)-|g_2|^2-|h_2|^2\Big], \\
J_4 &= \frac{\sqrt{2}s\beta_l^2}{m_{\mathrm{K}^*}}\Big[E_{\mathrm{K}^*}\big(|g_2|^2+|h_2|^2\big) \\
&\quad +p_{\mathrm{K}^*}^2(s)^{1/2}2\mathrm{Re}(g_2 g_3^*+h_2 h_3^*)\Big], \\
J_5 &= -\frac{\sqrt{8}p_{\mathrm{K}^*}(s)^{3/2}\beta_\ell}{m_{\mathrm{K}^*}}\Big[E_{\mathrm{K}^*}\mathrm{Re}(g_1 h_2^*+g_2 h_1^*) \\
&\quad +2p_{\mathrm{K}^*}^2 s^{1/2}\mathrm{Re}(g_1 h_3^*+g_3 h_1^*)\Big], \\
J_6^s &= -4p_{\mathrm{K}^*}(s)^{3/2}\beta_\ell\Big[\mathrm{Re}(g_1 h_2^*+g_2 h_1^*)\Big], \\
J_7 &= \frac{\sqrt{32}p_{\mathrm{K}^*}^2(s)^{3/2}\beta_\ell}{m_{\mathrm{K}^*}}\Big[\mathrm{Im}(g_2 h_3^*+g_3^* h_2)\Big],
\end{aligned}
$$

$$
\begin{aligned}
J_8 &= \frac{\sqrt{2}p_{\rm K^*}(s)^{3/2}\beta_l^2}{m_{\rm K^*}}\Big[E_{\rm K^*}{\rm Im}(g_1^*g_2{+}h_1^*h_2)\\
&\quad +2p_{\rm K^*}^2 s^{1/2}{\rm Im}(g_1^*g_3{+}h_1^*h_3)\Big],\\
J_9 &= 2p_{\rm K^*}(s)^{3/2}\beta_l^2\Big[{\rm Im}(g_1g_2^*{+}h_2h_1^*)\Big], \qquad \text{(A1)}
\end{aligned}
$$

where $g_i(h_i)$, $i=1,\cdots,3$ are the auxiliary functions and are given as follows:

$$
\begin{aligned}
h_1 &= \frac{4m_b}{s}\mathcal{T}_\perp{+}\frac{2}{M_{\rm B}{+}m_{\rm K^*}}C_9^{\rm tot}V(s),\\
g_1 &= \frac{2}{M_{\rm B}{+}m_{\rm K^*}}C_{10}^{\rm tot}V(s),\\
h_2 &= -(M_{\rm B}{+}m_{\rm K^*})C_9^{\rm tot}A_1(s)\\
&\quad -\frac{4m_b\big(m_{\rm B}^2{-}m_{\rm K^*}^2\big)}{s}\frac{E_{\rm K^*}}{M_{\rm B}}\mathcal{T}_\perp,\\
g_2 &= -(M_{\rm B}{+}m_{\rm K^*})A_1(s)C_{10}^{\rm tot},\\
h_3 &= \frac{A_2}{M_{\rm B}{+}m_{\rm K^*}}C_9^{\rm tot}\\
&\quad +\frac{2m_b}{s}\left[\frac{s(\mathcal{T}_\perp{+}\mathcal{T}_\parallel)}{m_{\rm B}^2{-}m_{\rm K^*}^2}{+}\frac{2E_{\rm K^*}}{M_{\rm B}}\mathcal{T}_\perp\right],\\
g_3 &= \frac{A_2}{M_{\rm B}{+}m_{\rm K^*}}C_{10}^{\rm tot}, \qquad \text{(A2)}
\end{aligned}
$$

$$
\begin{aligned}
E_{\rm K^*} &= \frac{m_{\rm B}^2{-}m_{\rm K^*}^2{-}s}{2\sqrt{s}}, \quad p_{\rm K^*}{=}\sqrt{E_{\rm K^*}^2{-}m_{\rm K^*}^2},\\
\beta_\ell &= \sqrt{1{-}\frac{4m_\ell^2}{s}}, \qquad \text{(A3)}
\end{aligned}
$$

and $\mathrm{a}_0 = \frac{E_{\rm K^*}}{m_{\rm K^*}}\frac{\xi_\parallel}{\Delta_\parallel}$ where $\Delta_\parallel$ is given in Appendix B in Eq. (B1).

Traditionally, the J's are given in terms of transversity amplitudes $A_{0,\parallel,\perp}$ but we have written them in terms of $g_i(h_i)$ functions given in Eq. (A2). The $A_{0,\parallel,\perp}$ are related with $g_i(h_i)$ as follows:

$$
\begin{aligned}
A_0^{L,R} &= \frac{\mathcal{N}}{m_{\rm K^*}}\Big[E_{k^*}(h_2{\mp}g_2){+}2p_{k^*}^2\sqrt{s}(h_3{\mp}g_3)\Big],\\
A_\parallel^{L,R} &= \sqrt{2}\mathcal{N}\big[h_2{\mp}g_2\big], \quad A_\perp^{L,R}{=}\sqrt{2s}\mathcal{N}p_{k^*}\big[h_1{\mp}g_1\big], \qquad \text{(A4)}
\end{aligned}
$$

where $\mathcal{N}{=}\alpha G_F|V_{\rm tb}V_{\rm ts}^*|\sqrt{\frac{s\beta_\ell p_{\rm K^*}}{3{\cdot}2^{10}\pi^5 m_{\rm B}^3}}$. Our expressions for the J's are consistent with the literature, for example as given in Refs. [14, 50].

The values of the Wilson coefficients at NNLO, Z′ parameters and other input parameters are listed in Tables A1, A2 and A3, respectively.

Table A1. Values of Wilson coefficients at $\mu_b{=}4{\cdot}8$.

$C_1(\mu_b)$	$C_2(\mu_b)$	$C_3(\mu_b)$	$C_4(\mu_b)$	$C_5(\mu_b)$	$C_6(\mu_b)$	$C_7^{\rm eff}(\mu_b)$	$C_8^{\rm eff}(\mu_b)$	$C_9(\mu_b)$	$C_{10}(\mu_b)$
-0.2632	1.0111	-0.0055	-0.0806	0.0004	0.0009	-0.2923	-0.1663	4.0749	-4.3085

Table A2. Numerical values of the Z′ parameters [42, 43]..

	$\lvert\mathcal{B}_{\rm sb}\rvert{\times}10^{-3}$	$\phi_{\rm sb}$(degree)	$S_{\ell\ell}^{LR}{\times}10^{-2}$	$D_{\ell\ell}^{LR}{\times}10^{-2}$
$\mathcal{S}1$	1.09±0.22	−72±7	−2.8±3.9	−6.7±2.6
$\mathcal{S}2$	2.20±0.15	−82±4	−1.2±1.4	−2.5±0.9
$\mathcal{S}3$	4.0±1.5	150±10 or (−150±10)	0.8	−2.6

Table A3. Values of input parameters.

$\alpha_{em}(M_Z){=}1/128.940$	[55]	$\alpha_s(M_Z){=}0.1184{\pm}0.0007$	[56]
$m_e{=}0.51099{\times}10^{-3}$ GeV	[56]	$m_\mu{=}0.10565837$ GeV	[56]
$m_{\rm B}{=}5.27950$ GeV	[56]	$m_{\rm K^*}{=}0.89594$ GeV	[56]
$m_b^{1S}{=}4.68{\pm}0.03$ GeV	[57]	$m_s{=}0.095{\pm}0.005$ GeV	[56]
$m_c^{\overline{MS}}(m_c){=}1.27{\pm}0.09$ GeV	[56]		
$\lvert V_{\rm tb}\rvert{=}0.999139{\pm}0.000045$	[56]	$\lvert V_{\rm ts}\rvert{=}(40.5{\pm}0.11){\cdot}10^{-3}$	[56]
$f_{\rm B}{=}194{\pm}10$ MeV	[60]	$\lambda_{\rm B}{=}460{\pm}110$ MeV	[59]
$f_{\rm K^*,||}{=}220{\pm}5$ MeV	[58]	$f_{\rm K^*,\perp}{=}185{\pm}9$ MeV	[58]
$a_{1,||}{=}0.03{\pm}0.03$	[33]	$a_{2,||}{=}0.08{\pm}0.06$	[33]
$a_{1,\perp}{=}0.03{\pm}0.03$	[33]	$a_{2,\perp}{=}0.08{\pm}0.06$	[33]

Appendix B

The expression of $\Delta_\parallel$, which appears in the definition of a_0 below Eq. (A3), is written as follows:

$$\Delta_\parallel(s) = 1+\frac{\alpha_s C_F}{4\pi}[(2L-2) - \frac{2s}{E_{\rm K^*}^2}\frac{\pi^2 f_{\rm B} f_{\rm K^*\parallel}\lambda_{B+}^{-1}}{N_c m_{\rm B}(E_{\rm K^*}/m_{\rm K^*})\xi_\parallel(s)}\int_0^1\frac{{\rm d}u}{\bar{u}}\Phi_{\bar{\rm K}^*,\parallel}\Bigg], \tag{B1}$$

and contributes only for massive leptons. The light-cone distribution amplitude (LCDA) $\Phi_{\bar{\rm K}^*,a}$ for transversely ($a=\perp$) and longitudinally ($a=\parallel$) polarized $\rm K^*$ can be written as [40, 51]:

$$\Phi_{\bar{\rm K}^*,a} = 6u(1-u)\{1+a_1\left(\bar{\rm K}^*\right)_a C_1^{(3/2)}(2u-1) + a_2\left(\bar{\rm K}^*\right)_a C_2^{(3/2)}(2u-1)\}, \tag{B2}$$

where $L=-(m_b^2-s)/s\ln\left(1-s/m_b^2\right)$ and $a_i\left(\bar{\rm K}^*\right)_a$ are the Gegenbauer coefficients. The moments are

$$\lambda_{\rm B,+}^{-1} = \int_0^\infty {\rm d}\omega\frac{\Phi_{\rm B,+}(\omega)}{\omega},$$
$$\lambda_{\rm B,-}^{-1} = \int_0^\infty {\rm d}\omega\frac{\Phi_{\rm B,-}(\omega)}{\omega-s/m_{\rm B}-i\epsilon}$$

where $\Phi_{\rm B,\pm}$ are the two B-meson light-cone distribution amplitudes [40]. The $\lambda_{\rm B,-}^{-1}(s)$ can be expressed as:

$$\lambda_{\rm B,-}^{-1}(s)=\frac{{\rm e}^{-s/(m_{\rm B}\omega_0)}}{\omega_0}[-\boldsymbol{Ei}(s/m_{\rm B}\omega_0)+{\rm i}\pi],$$

where $\omega_0=2(m_{\rm B}-m_b)$. The ξ_a are the universal form factors,

$$\xi_\perp = \frac{m_{\rm B}}{m_{\rm B}+m_{\rm K^*}}V$$
$$\xi_\parallel = \frac{m_{\rm B}+m_{\rm K^*}}{2E_{\rm K^*}}A1-\frac{m_{\rm B}-m_{\rm K^*}}{m_{\rm B}}A2. \tag{B3}$$

The $\rm B\to K^*$ matrix elements in the heavy quark limit depend on four independent functions $\mathcal{T}_a^\pm$ ($a=\perp,\parallel$). In the low s, ($1.0<s<6.0{\rm GeV}^2$), the invariant amplitudes $\mathcal{T}_{\perp,\parallel}$ at NLO within QCDf are given in [38, 40, 50],

$$\mathcal{T}_a = \xi_a C_a+\frac{\pi^2}{N_c}\frac{f_{\rm B}f_{\rm K^*,a}}{m_{\rm B}}\Xi_a\sum_\pm\int\frac{{\rm d}\omega}{\omega} \times\Phi_{\rm B,\pm}(\omega)\int_0^1{\rm d}u\Phi_{\rm K^*,a}(u)T_{a,\pm}(u,\omega), \tag{B4}$$

where $\Xi_\perp\equiv 1$, $\Xi_\parallel\equiv m_{\rm K^*}/E_{\rm K^*}$ and the factorization scale $\mu_f=\sqrt{m_b\Lambda_{QCD}}$. The coefficient functions C_a and hard scattering functions $T_{a,\pm}$ are written as:

$$C_a = C_a^{(0)}+\frac{\alpha_s(\mu_b)C_F}{4\pi}C_a^{(1)}$$
$$T_{a,\pm} = T_{a,\pm}^{(0)}(u,\omega)+\frac{\alpha_s(\mu_f)C_F}{4\pi}T_{a,\pm}^{(1)}(u,\omega). \tag{B5}$$

The form factor terms $C_a^{(0)}$ at LO are:

$$C_\perp^{(0)}=C_7^{\rm eff}+\frac{s}{2m_b m_{\rm B}}Y(s), \quad \text{and} \quad C_\parallel^{(0)}=-C_7^{\rm eff}-\frac{m_{\rm B}}{2m_b}Y(s).$$

$$Y(s)=h(s,m_c)\left(\frac{4}{3}C_1+C_2+6C_3+60C_5\right) -\frac{1}{2}h(s,m_b^{\rm pole})\left(7C_3+\frac{4}{3}C_4+76C_5+\frac{64}{3}C_6\right) -\frac{1}{2}h(s,0)\left(C_3+\frac{4}{3}C_4+16C_5+\frac{64}{3}C_6\right) +\frac{4}{3}C_4+\frac{64}{9}C_5+\frac{64}{27}C_6,$$

where $h(s,m_q)$ is the well-known fermionic loop function. The coefficients $C_a^{(1)}$ at NLO are divided into a factorizable and a non-factorizable part as

$$C_a^{(1)}=C_a^{(f)}+C_a^{(nf)}. \tag{B6}$$

At NLO the factorizable correction reads [40, 52],

$$C_\perp^{(f)} = C_7^{\rm eff}\left(\ln\frac{m_b^2}{\mu^2}-L+\Delta M\right)$$
$$C_\parallel^{(f)} = -C_7^{\rm eff}\left(\ln\frac{m_b^2}{\mu^2}+2L+\Delta M\right).$$

The non-factorizable corrections are,

$$C_F C_\perp^{(nf)} = -\bar{C}_2F_2^{(7)}-C_8^{\rm eff}F_8^{(7)}-\frac{s}{2m_b m_{\rm B}} \times\left[\bar{C}_2F_2^{(9)}+2\bar{C}_1\left(F_1^{(9)}+\frac{1}{6}F_2^{(9)}\right)+C_8^{\rm eff}F_8^{(9)}\right],$$
$$C_F C_\parallel^{(nf)} = \bar{C}_2F_2^{(7)}+C_8^{\rm eff}F_8^{(7)}+\frac{m_{\rm B}}{2m_b} \times\left[\bar{C}_2F_2^{(9)}+2\bar{C}_1\left(F_1^{(9)}+\frac{1}{6}F_2^{(9)}\right)+C_8^{\rm eff}F_8^{(9)}\right],$$

where ΔM depends on the mass renormalization convention for m_b. These corrections are obtained from the matrix elements of four-quark and chromomagnetic dipole operators [40] that are embedded in $F_{1,2}^{(7,9)}$ and $F_8^{(7,9)}$ [53, 54].

At LO the hard-spectator scattering term $T_{a,\pm}^{(0)}(u,\omega)$ from the weak annihilation diagram is [40]:

$$T_{\perp,+}^{(0)}(u,\omega)=T_{\perp,-}^{(0)}(u,\omega)=T_{\parallel,+}^{(0)}(u,\omega)=0,$$

$$T_{\parallel,-}^{(0)}(u,\omega)=-e_q\frac{m_{\rm B}\omega}{m_{\rm B}\omega-s-{\rm i}\epsilon}\frac{4m_{\rm B}}{m_b}\left(\bar{C}_3+3\bar{C}_4\right).$$

The contributions to $T_a^{(1)}$ at NLO also contain a factorizable as well as non-factorizable part,

$$T_a^{(1)}=T_a^{(f)}+T_a^{(nf)}. \tag{B7}$$

Including $\mathcal{O}(\alpha_s)$ corrections, the factorizable terms to $T_{a,\pm}^{(1)}$ are given by [40, 52]:

$$T_{\perp,+}^{(f)}(u,\omega) = C_7^{\rm eff}\frac{2m_{\rm B}}{\bar{u}E_{\rm K^*}}, \quad T_{\parallel,+}^{(f)}(u,\omega)=C_7^{\rm eff}\frac{4m_{\rm B}}{\bar{u}E_{\rm K^*}}$$
$$T_{\perp,-}^{(f)}(u,\omega) = T_{\parallel,-}^{(f)}(u,\omega)=0,$$

where $\bar{u}=1-u$. The non-factorizable correction comes through the matrix elements of four-quark operators and the chromomagnetic dipole operator:

$$\begin{aligned}
T_{\perp,+}^{(nf)}(u,\omega)=&-\frac{4e_dC_8^{\rm eff}}{u+\bar{u}s/m_{\rm B}^2}\\
&+\frac{m_{\rm B}}{2m_b}[e_ut_\perp(u,m_c)\left(\bar{C}_2+\bar{C}_4-\bar{C}_6\right)\\
&+e_dt_\perp(u,m_b)\left(\bar{C}_3+\bar{C}_4-\bar{C}_6-4m_b/m_{\rm B}\bar{C}_5\right)\\
&+e_dt_\perp(u,0)\bar{C}_3],\\
T_{\perp,-}^{(nf)}(u,\omega)=&0,\\
T_{\parallel,+}^{(nf)}(u,\omega)=&\frac{m_{\rm B}}{m_b}[e_ut_\parallel(u,m_c)\left(\bar{C}_2+\bar{C}_4-\bar{C}_6\right)\\
&+e_dt_\parallel(u,m_b)\left(\bar{C}_3+\bar{C}_4-\bar{C}_6\right)+e_dt_\parallel(u,0)\bar{C}_3],
\end{aligned}$$

$$\begin{aligned}
T_{\parallel,-}^{(nf)}(u,\omega)=&e_q\frac{m_{\rm B}\omega}{m_{\rm B}\omega-s-{\rm i}\epsilon}\Bigg[\frac{8C_8^{\rm eff}}{\bar{u}+us/m_{\rm B}^2}\\
&+\frac{6m_{\rm B}}{m_b}\Bigg(h\left(\bar{u}m_{\rm B}^2+us,m_c\right)\left(\bar{C}_2+\bar{C}_4+\bar{C}_6\right)\\
&+h\left(\bar{u}m_{\rm B}^2+us,m_b^{\rm pole}\right)\left(\bar{C}_3+\bar{C}_4+\bar{C}_6\right)\\
&+h\left(\bar{u}m_{\rm B}^2+us,0\right)\left(\bar{C}_3+3\bar{C}_4+3\bar{C}_6\right)\\
&-\frac{8}{27}\left(\bar{C}_3-\bar{C}_5-15\bar{C}_6\right)\Bigg)\Bigg].
\end{aligned}$$

The $t_a(u,m_q)$ functions are given by

$$\begin{aligned}
t_\perp(u,m_q)&=\frac{2m_{\rm B}}{\bar{u}E_{\rm K^*}}I_1(m_q)+\frac{s}{\bar{u}^2E_{\rm K^*}^2}\\
&\quad\times\left(B_0\left(\bar{u}m_{\rm B}^2+us,m_q\right)-B_0(s,m_q)\right),\\
t_\parallel(u,m_q)&=\frac{2m_{\rm B}}{\bar{u}E_{\rm K^*}}I_1(m_q)+\frac{\bar{u}m_{\rm B}^2+us}{\bar{u}^2E_{\rm K^*}^2}\\
&\quad\times\left(B_0\left(\bar{u}m_{\rm B}^2+us,m_q\right)-B_0(s,m_q)\right),
\end{aligned}$$

where B_0 and I_1 are

$$B_0(s,m_q)=-2\sqrt{4m_q^2/s-1}\arctan\frac{1}{\sqrt{4m_q^2/s-1}},$$

$$I_1(m_q)=1+\frac{2m_q^2}{\bar{u}(m_{\rm B}^2-s)}\left[L_1(x_+)+L_1(x_-)-L_1(y_+)-L_1(y_-)\right],$$

and

$$x_\pm=\frac{1}{2}\pm\left(\frac{1}{4}-\frac{m_q^2}{\bar{u}m_{\rm B}^2+us}\right)^{1/2},\quad y_\pm=\frac{1}{2}\pm\left(\frac{1}{4}-\frac{m_q^2}{s}\right)^{1/2},$$

$$L_1(x)=\ln\frac{x-1}{x}\ln(1-x)-\frac{\pi^2}{6}+Li_2\left(\frac{x}{x-1}\right).$$

References

1 S. Descotes-Genon, J. Matias, M. Ramon, and J. Virto, JHEP, **1301**: 048 (2013) doi:10.1007/JHEP01(2013)048 [arXiv:1207.2753 [hep-ph]]
2 S. Descotes-Genon, T. Hurth, J. Matias, and J. Virto, JHEP, **1305**: 137 (2013), [arXiv:1303.5794 [hep-ph]]
3 **LHCb** Collaboration, PRL, **111** (2013) 191801 [arXiv:1308.1707 [hep-ex]]
4 R. Aaij et al (LHCb Collaboration), JHEP, **1602** (2016) 104 [arXiv:1512.04442 [hep-ex]]
5 A. Bharucha, D. M. Straub, and R. Zwicky, JHEP, **1608**: 098 (2016) doi:10.1007/JHEP08(2016)098 [arXiv:1503.05534 [hep-ph]]
6 A. Abdesselam et al (Belle Collaboration), arXiv:1604.04042 [hep-ex]
7 S. Wehle et al (Belle Collaboration), arXiv:1612.05014 [hep-ex]
8 ATLAS Collaboration, *Angular analysis of* $B_d^0\to K^*\mu^+\mu^-$ *decays in pp collisions at* $\sqrt{s}$=8 *TeV with the ATLAS detector*: Tech. Rep. ATLAS-CONF-2017-023, CERN, Geneva, 2017
9 CMS Collaboration, *Measurement of the* P_1 *and* P_5' *angular parameters of the decay* $B^0\to K^{*0}\mu^+\mu^-$ *in proton-proton collisions at* $\sqrt{s}$ = 8 TeV: Tech. Rep. CMS-PAS-BPH-15-008, CERN, Geneva, 2017
10 CMS Collaboration, V. Khachatryan et al, Phys. Lett. B, **753**: 424–448 (2016), [arXiv:1507.08126]
11 W. Altmannshofer, C. Niehoff, P. Stangl, and D. M. Straub, arXiv:1703.09189 [hep-ph]
12 LHCb Collaboration, Phys. Rev. Lett., **113** (2014) 151601 [arXiv:1406.6482 [hep-ex]]
13 R. Aaij et al (LHCb Collaboration), JHEP, **1509** (2015) 179 [arXiv:1506.08777 [hep-ex]]
14 J. Matias, F. Mescia, M. Ramon, and J. Virto, JHEP, **1204** (2012) 104, arXiv:1202.4266 [hep-ph]
15 B. Capdevila, S. Descotes-Genon, L. Hofer, and J. Matias, arXiv:1701.08672 [hep-ph]
16 V. G. Chobanova, T. Hurth, F. Mahmoudi, D. Martinez Santos, and S. Neshatpour, arXiv:1702.02234 [hep-ph]
17 S. Descotes-Genon, J. Matias, and J. Virto, Phys. Rev. D, **88**: 074002 (2013) [arXiv:1307.5683 [hep-ph]]; W. Altmannshofer and D. M. Straub, Eur. Phys. J. C, **73** (2013) 2646] [arXiv:1308.1501 [hep-ph]]; F. Mahmoudi, S. Neshatpour, and J. Virto, Eur. Phys. J. C, **74** (2014) 6, 2927 [arXiv:1401.2145 [hep-ph]]; S. Jager and J. Martin Camalich, JHEP, **1305** (2013) 043 [arXiv:1212.2263 [hep-ph]]; G. Hiller and M. Schmaltz, Phys. Rev. D, **90** (2014) 054014 [arXiv:1408.1627 [hep-ph]]; A. J. Buras, F. De Fazio, and J. Girrbach-Noe, JHEP, **1408** (2014) 039 [arXiv:1405.3850 [hep-ph]]; R. Gauld, F. Goertz, and U. Haisch, JHEP, **1401** (2014) 069 [arXiv:1310.1082 [hep-ph]];
18 U. Egede, T. Hurth, J. Matias, M. Ramon, and W. Reece, JHEP, **1010**: 056 (2010) [arXiv:1005.0571 [hep-ph]]
19 W. Altmannshofer, and D. M. Straub, Eur. Phys. J. C, **75**(8): 382 (2015) [arXiv:1411.3161 [hep-ph]]
20 F. Beaujean, C. Bobeth, and D. van Dyk, Eur. Phys. J. C, **74**: 2897 (2014) Erratum: [Eur. Phys. J. C, **74**: 3179 (2014)] [arXiv:1310.2478 [hep-ph]]
21 T. Hurth, and F. Mahmoudi, JHEP, **1404**: 097 (2014) [arXiv:1312.5267 [hep-ph]]; T. Hurth and F. Mahmoudi, Nucl. Part. Phys. Proc., **263-264**: 38 (2015) [arXiv:1411.2786 [hep-ph]]
22 S. Jager and J. Martin Camalich, Phys. Rev. D, **93**(1): 014028 (2016) [arXiv:1412.3183 [hep-ph]]
23 B. Allanach, F. S. Queiroz, A. Strumia, and S. Sun, Phys. Rev. D, **93**(5): 055045 (2016) [arXiv:1511.07447 [hep-ph]]
24 A. Crivellin, L. Hofer, J. Matias, U. Nierste, S. Pokorski, and J. Rosiek, Phys. Rev. D, **92**(5): 054013 (2015) [arXiv:1504.07928 [hep-ph]]

25 S. J盲ger, K. Leslie, M. Kirk, and A. Lenz, arXiv:1701.09183 [hep-ph]
26 S. Descotes-Genon, J. Matias, and J. Virto, Phys. Rev. D, **88**: 074002 (2013) [arXiv:1307.5683 [hep-ph]]
27 W. Altmannshofer and D. M. Straub, Eur. Phys. J. C, **73**: 2646 (2013) [arXiv:1308.1501 [hep-ph]]
28 R. Gauld, F. Goertz, and U. Haisch, Phys. Rev. D, **89**: 015005 (2014) [arXiv:1308.1959 [hep-ph]]
29 R. Gauld, F. Goertz, and U. Haisch, JHEP, **1401**: 069 (2014) [arXiv:1310.1082 [hep-ph]]
30 A. J. Buras, F. De Fazio, and J. Girrbach, JHEP, **1402**: 112 (2014) [arXiv:1311.6729 [hep-ph]]
31 A. J. Buras and J. Girrbach, JHEP, **1312**: 009 (2013) [arXiv:1309.2466 [hep-ph]]
32 B. Capdevila, S. Descotes-Genon, J. Matias, and J. Virto, JHEP, **1610**: 075 (2016) [arXiv:1605.03156 [hep-ph]]
33 P. Ball and R. Zwicky, Phys. Rev. D, **71**: 014029 (2005) [hep-ph/0412079]
34 P. Langacker and M. Plumacher, Phys. Rev. D, **62**: 013006 (2000) [hep-ph/0001204]
35 Q. Chang and Y. H. Gao, Nucl. Phys. B, **845**: 179 (2011) [arXiv:1101.1272 [hep-ph]]; Y. Li, J. Hua, and K. C. Yang, Eur. Phys. J. C, **71**: 1775 (2011) [arXiv:1107.0630 [hep-ph]]
36 K. Cheung, C. W. Chiang, N. G. Deshpande, and J. Jiang, Phys. Lett. B, **652**: 285 (2007) [hep-ph/0604223]; C. H. Chen and H. Hatanaka, Phys. Rev. D, **73**: 075003 (2006) [hep-ph/0602140]; C. W. Chiang, N. G. Deshpande, and J. Jiang, JHEP, **0608**: 075 (2006) [hep-ph/0606122]
37 V. Barger, C. W. Chiang, P. Langacker, and H. S. Lee, Phys. Lett. B, **580**: 186 (2004) [hep-ph/0310073]; V. Barger, L. Everett, J. Jiang, P. Langacker, T. Liu, and C. Wagner, Phys. Rev. D, **80**: 055008 (2009) [arXiv:0902.4507 [hep-ph]]; R. Mohanta and A. K. Giri, Phys. Rev. D, **79**: 057902 (2009) [arXiv:0812.1842 [hep-ph]]; J. Hua, C. S. Kim, and Y. Li, Eur. Phys. J. C, **69**: 139 (2010) [arXiv:1002.2531 [hep-ph]]
38 C. Bobeth, G. Hiller, and G. Piranishvili, JHEP, **0807**: 106 (2008) [arXiv:0805.2525 [hep-ph]]
39 M. Beneke and T. Feldmann, Nucl. Phys. B, **592**: 3 (2001) [hep-ph/0008255]
40 M. Beneke, T. Feldmann, and D. Seidel, Nucl. Phys. B, **612**: 25 (2001) [hep-ph/0106067]
41 S. Descotes-Genon, L. Hofer, J. Matias, and J. Virto, JHEP, **1606**: 092 (2016) [arXiv:1510.04239 [hep-ph]]
42 Q. Chang, X. Q. Li, and Y. D. Yang, JHEP, **1002**: 082 (2010) [arXiv:0907.4408] [hep-ph]
43 M. Bona et al (UTfit collaboration), PMC Phys. a **3** (2009) [arXiv:0803.0659 [hep-ph]]; M. Bona et al, arXiv: 0906.0953 [hep-ph]
44 X.-Q. Li, Y.-M. Li, G.-R.Lin, JHEP, **1205**: 049 (2012) [arXiv:1204.5250 [hep-ph]]
45 M. Iwasaki et al (Belle Collaboration), Phys. Rev. D, **72**: 092005 (2005)
46 J. P. Lees et al (BaBar Collaboration), arXiv:1204.3993 [hep-ex]
47 R. Aaij et al (LHCb Collaboration), Phys. Rev. Lett., **108**: 181806 (2012)
48 R. Aaij et al (LHCb Collaboration), Phys. Rev. Lett., **108**: 231801 (2012)
49 T. M. Aliev, K. Azizi, and M. Savci, Phys. Letters B, **718**: 566 (2012)
50 W. Altmannshofer, P. Ball, A. Bharucha, A. J. Buras, D. M. Straub, and M. Wick, JHEP, **0901**: 019 (2009) [arXiv:0811.1214 [hep-ph]]
51 P. Ball and M. Boglione, Phys. Rev. D, **68**: 094006 (2003) [hep-ph/0307337]
52 M. Beneke, T. Feldmann, and D. Seidel, Eur. Phys. J. C, **41**: 173 (2005) [hep-ph/0412400]
53 H. H. Asatryan, H. M. Asatrian, C. Greub, and M. Walker, Phys. Rev. D, **65**: 074004 (2002) [hep-ph/0109140]; H. H. Asatrian, H. M. Asatrian, C. Greub, and M. Walker, Phys. Lett. B, **507**: 162 (2001) [hep-ph/0103087]
54 C. Greub, V. Pilipp, and C. Schupbach, JHEP, **0812**: 040 (2008) [arXiv:0810.4077 [hep-ph]]
55 M. Misiak et al, Phys. Rev. Lett., **98**: 022002 (2007) [hep-ph/0609232]
56 K. A. Olive et al (Particle Data Group), Chin. Phys. C, **38**: 090001 (2014)
57 C. W. Bauer, Z. Ligeti, M. Luke, A. V. Manohar, and M. Trott, Phys. Rev. D, **70**: 094017 (2004) [hep-ph/0408002]
58 P. Ball, G. W. Jones, and R. Zwicky, Phys. Rev. D, **75**: 054004 (2007) [hep-ph/0612081]
59 P. Ball and R. Zwicky, JHEP, **0604**: 046 (2006) [hep-ph/0603232]
60 F. Mahmoudi, S. Neshatpour, and J. Orloff, JHEP, **1208**: 092 (2012) [arXiv:1205.1845 [hep-ph]]